Fuel 409 (2026) 137896

Contents lists available at ScienceDirect

Fuel

journal homepage: www.elsevier.com/locate/fuel

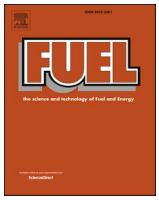

Full Length Article

AsPyCC: Post-combustion carbon capture design through Aspen Plus® & Python

Fernando Zea [a,b,*], Christopher Varela [b,c], Kyle V. Camarda [a]

[a] Department of Chemical and Petroleum Engineering, University of Kansas, 1530 West 15th Street, Lawrence 66045 KS, United States
[b] Facultad de Ciencias Naturales y Matemáticas, Escuela Superior Politécnica del Litoral, ESPOL, Campus Gustavo Galindo km. 30.5 Vía Perimetral, Guayaquil 090902, Ecuador
[c] German Aerospace Center (DLR), Institute of Networked Energy Systems, Carl-von-Ossietzky-Straße 15, Oldenburg 26129, Germany

ARTICLE INFO

Keywords:
Carbon capture
Process simulation
Techno-economic analysis
Process design framework

ABSTRACT

A novel AsPyCC framework is introduced to conduct techno-economic evaluations of post-combustion carbon capture (PCC) units. The framework is demonstrated across seven industrial sectors, represented with different flue gas compositions. The automated framework integrates design, sizing, and simulation of PCC units in Aspen Plus® via Python, ensuring compliance with industry standards, while reducing the design effort as compared to traditional process synthesis methods. This is possible because design heuristics were integrated in the tool, namely target loadings, capture rate, geometrical relations, flooding percentage, etc. For testing the capabilities of the tool, a total of 35 PCC units considering an ammonia-based solvent were designed targeting 90 ± 5 % CO_2 capture rate (CCR), 0.12 lean loading, 5 wt% NH_3 in the make-up solvent, and different flue gas compositions. The results demonstrated an average CCR of 89.70 %, with solvent losses below 10 %, and regeneration energy values within literature-reported ranges. An extended techno-economic sensitivity analysis was conducted to assess the influence of NH_3 sourcing pathways and plant capacity on the total operating cost and carbon capture cost. Results showed that most cases remained within the same order of magnitude as current carbon market prices, reinforcing the economic viability of the proposed PCC configurations. This evaluation, incorporating relevant metrics such as the industry sector index (ISI), capacity sector index (CSI), and available CO_2 score index (ACSI), identified cost-effective carbon capture scenarios. Clustering analysis, supported by principal component analysis (PCA), revealed three distinct groups of industrial cases based on economic and operational characteristics. Cement plants, natural gas and coal-fired power plants exhibited the highest ISI scores, with 200 t/h to 300 t/h plant capacities being identified as suitable for PCC implementation. The ASCI analysis determined that CO_2 concentrations between 17–19 % and 11–17 % were most suitable for 200 t/h and 300 t/h plants, respectively.

1. Introduction

Greenhouse gas mitigation technologies have garnered significant attention in response to escalating concerns about global warming [1]. In 2018, the U.S. EPA reported that 76 % of industrial carbon dioxide (CO_2) emissions in the United States originated from fossil fuel combustion, with major contributors being power plants, oil and gas operations, chemical manufacturing facilities, and petroleum refineries [2]. Carbon capture (CC) technologies play a crucial role in addressing emissions from these hard-to-decarbonize sectors, with Post-Combustion Capture (PCC) standing out as a mature and retrofittable approach for CO_2 removal from flue gases [3].

The dominant commercial PCC technology involves chemical absorption using different solvents such as alkanolamines, alkali solvents, ammonia (NH_3), ionic liquids (ILs), phase change solvents, amino acids, and sterically hindered amines [4]. Monoethanolamine (MEA) is the most widely used solvent for PCC due to its high CO_2 capture rate and selectivity at low partial pressures. However, its application presents several drawbacks, including high energy requirements for regeneration, potential equipment corrosion, and significant solvent losses due to oxidative degradation [5–8].

Recently, NH_3 has gained attention as an alternative solvent due to its lower regeneration energy requirements, ability to simultaneously capture CO_2, sulfur dioxide (SO_2), and nitrogen oxides (NO_x), and its

* Corresponding author.

https://doi.org/10.1016/j.fuel.2025.137896
Received 14 September 2025; Received in revised form 7 November 2025; Accepted 1 December 2025
Available online 5 December 2025

cost-effectiveness compared to amines [9]. Additionally, ammonia offers a higher CO_2 absorption capacity, low corrosiveness, and low cost [10]. However, its implementation requires additional energy and capital investment to manage solvent evaporation and recovery, owing to its high volatility [11].

During typical operation, the aqueous NH_3 solvent is introduced at the top of the absorption column, flowing downward over the packing material while absorbing CO_2 from the flue gas entering at the column's base [12]. This countercurrent flow results in the release of CO_2-free gas at the top of the column and the generation of a CO_2-rich solution at the bottom [13]. The CO_2-rich solution is then routed through a cross-heat exchanger, where it is preheated by the recycled lean solution from the stripper column's bottom. Following this, the solution enters through the top of the stripper column where heat is applied to reverse the CO_2 absorption reactions [14], producing a bottom liquid stream primarily consisting of aqueous NH_3 and a top vapor stream predominantly containing CO_2. The regenerated CO_2 is subsequently directed to a compression train for further processing [15].

Captured CO_2 can be injected at high pressure into geological formations or offshore reservoirs, or it can be converted into value-added chemical feedstocks, contributing to environmental mitigation and sustainable development [16,17]. CO_2 serves as a valuable feedstock for various industrial processes, including methanol and fertilizer production [18–20], biomass gasification [21], dimethyl ether synthesis [22], and Fischer-Tropsch (FT) synthetic fuels production [23], among others. As a retrofittable technology, PCC presents an effective approach for integrating carbon capture into existing industrial processes [24,25], meeting the demands of their operations, enhancing both economic and environmental benefits [26–28].

Due to the complexity of the reactive absorption-stripping process and the variability among emitting facilities in terms of plant size, flue gas composition, capacity, and geographical location, a tailored process design and modeling approach is essential for developing a PCC unit that aligns with the specific characteristics of the flue gas source [29,30]. Therefore, this work focuses on the development of a process design and sizing framework for PCC units. The framework uses a rate-based approach to accurately represent simultaneous mass and energy transfer, incorporating diffusion in both phases as well as equilibrium and kinetic reactions [29] within the Aspen Plus® simulator. The novelty of this work lies in the development of a Python scheme that automates the design and sizing of PCC units, which aids the process synthesis task. The proposed framework integrates process design heuristics, specific operating conditions, and target performance metrics to ensure the units meet desired efficiency standards. Additionally, it enables the evaluation of various flue gas compositions, allowing for an accurate assessment of CO_2 capture potential across different industrial sectors.

2. Methodology

2.1. PCC unit: Basis of design

The units operate with a fixed inlet temperature of 50 °C and a pressure of 101 kPa. Pretreatment and cooling are assumed to occur in a Direct Contact Cooler (DCC), which is not included in the design algorithm. A 5 wt% aqueous NH_3 solution with a CO_2 loading of 0.12 (apparent mol CO_2/apparent mol NH_3) is introduced into the absorber from the top, while flue gas enters from the bottom. CO_2 is absorbed by the lean solvent, forming a CO_2-rich solution, which is then preheated in a cross-heat exchanger before further conditioning in another heat exchanger prior to entering the stripper. In the stripper, the rich solvent is heated in a reboiler, generating CO_2 and water vapors, which exit at the top. A condenser cools the vapor stream, separating CO_2 from water.

The CO_2 product stream is assumed to be sent to a compression train for further chemical upgrading, while the condensed water is returned to the stripper. The hot lean solvent exiting the stripper bottom transfers heat to the rich solvent in the cross-heat exchanger before being mixed with NH_3 make-up solution and cooled before re-entering the absorber. A summary of the general PCC unit and operating conditions are provided in Table 1, and a general process layout is illustrated in Fig. 1.

The vapor–liquid equilibrium and thermodynamic properties are computed using the Electrolyte-NRTL method and the Redlich-Kwong equation of state (ENRTL-RK) [31]. The Electrolyte-NRTL method is used for liquid-phase property calculations due to its reliability in process modeling and simulation. This approach depends solely on binary interaction parameters and maintains consistency by applying the mole fraction concentration scale for short-range local composition interactions. For the vapor phase, the Redlich-Kwong equation of state is utilized to determine thermodynamic properties, ensuring accurate representation of phase behavior [31,32]. The main chemical reactions involved in the process are summarized in Table 2 [33]. The simulation is conducted in Aspen Plus®, utilizing the rate-based RadFrac module for the absorber. The stripper operates based on the chemical equilibrium of the species [15,34]. Both columns employ MELLAPK 250Y as the internal packing material. The design parameters of the absorber and stripper columns are provided in Table 3.

2.2. Python-Aspen Plus® COM-connection: AsPyCC framework

The presented framework for the design and simulation of PCC units is implemented in Python via a Component Object Model (COM) interface, enabling automated and iterative process analysis. This framework facilitates the systematic evaluation of column dimensions and process variables to ensure they meet predefined performance criteria. The Python-based structure supports the incorporation of process heuristics and specific operational constraints. Within this framework, the absorber is configured to achieve a target CO_2 capture efficiency while maintaining hydraulic integrity, avoiding excessive column flooding and respecting a maximum allowable diameter. The stripper and make-up stream configurations are designed to ensure that the CO_2 loading in the recycle stream matches that of the lean solvent.

The AsPyCC framework is not limited to NH_3-based systems; it can also be applied to other solvent classes such as amines (e.g., MEA, diethanolamine (DEA), methyldiethanolamine (MDEA), or blends like piperazine-methyldiethanolamine (PZ + MDEA)) and ILs. The key requirement for its implementation with alternative solvents lies in establishing the appropriate simulation environment, including the definition of components, thermodynamic model selection, and reaction specification. For amine-based systems, this setup is relatively straightforward since common amines are readily available in the Aspen Plus ® component database, and established templates for amine-based CO_2 capture processes already exist within the software [35–38]. The ENRTL-RK thermodynamic model is typically suitable for representing these systems, and reaction kinetics can be defined using well-documented parameters available in the literature [39–41].

Table 1
General operating conditions of the PCC unit.

Equipment	Parameter	Specification
Absorber	Flue gas inlet temperature	50 °C
	Flue gas inlet pressure	101 kPa
	Lean solvent inlet temperature	15 °C
	Lean solvent inlet pressure	101 kPa
	Lean solvent loading	0.12
Cross-heat exchanger	Exchanger side	Hot
	Specification	Temperature
	Value	50 °C
Heat-exchanger	Outlet temperature	135 °C
	Outlet pressure	500 kPa
Stripper	Pressure	500 kPa
Condenser	Temperature	30 °C
	Pressure	500 kPa
Cooler	Outlet temperature	15 °C
	Outlet pressure	101 kPa

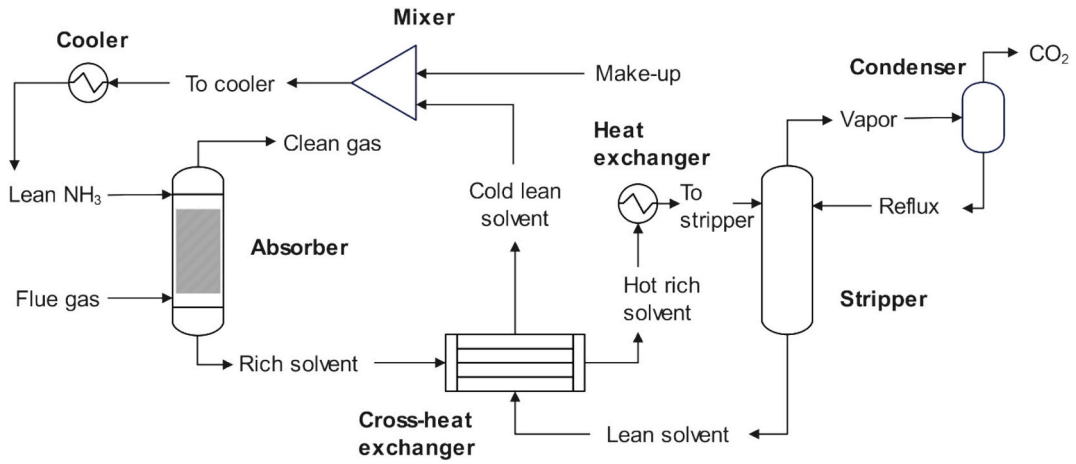

Fig. 1. PCC using aqueous NH_3 general flowsheet.

Table 2
Kinetic, equilibrium, and salt reaction involved in the reactive capture process.

Type of reaction	Reaction
Equilibrium	$NH_3 + H_2O \leftrightarrow NH_4^+ + OH^-$
Equilibrium	$2H_2O \leftrightarrow H_3O^+ + OH^-$
Equilibrium	$HCO_3^- + H_2O \leftrightarrow H_3O^+ + CO_3^-$
Kinetic	$CO_2 + OH^- \rightarrow HCO_3^-$
Kinetic	$HCO_3^- \rightarrow CO_2 + OH^-$
Kinetic	$NH_3 + CO_2 + H_2O \rightarrow H_2NCOO^- + H_3O^+$
Kinetic	$H_2NCOO^- + H_3O^+ \rightarrow NH_3 + CO_2 + H_2O$
Salt formation	$NH_4HCO_3(S) \leftrightarrow NH_4^+ + HCO_3^-$

Table 3
Absorber and stripper design parameters.

Equipment	Parameter	Specification
Absorber	Calculation type	Rate-based
	Packing material	MELLAPK 250Y
	Reaction condition factor	0.9
	Film discretization option	Geometric
	Film discretization ratio	10
	Liquid phase film resistance	Discretize film
	Liquid phase number of discretization points	5
	Vapor phase film resistance	Consider film
	Mass transfer coefficient method	Brf-85
	Heat transfer coefficient method	Chilton and Colburn
	Interfacial area method	Brf-85
	Holdup correlation method	Brf-92
	Condenser	None
	Reboiler	None
Stripper	Calculation type	Equilibrium
	Packing material	MELLAPK 250Y
	Condenser	None
	Reboiler	Kettle

In contrast, the use of ionic liquids requires a more detailed initialization, as these compounds are not included in the Aspen Plus ® databases. ILs can be introduced either as pseudocomponents, by defining their molecular weight, normal boiling point, and density; or as user-defined conventional components if structural information is available [42,43]. These fundamental properties can be obtained experimentally or estimated using predictive methods reported in the literature [44]. Once defined, several thermodynamic models can be employed to represent ILs systems, with UNIFAC and COSMO-based methods being among the most widely used due to their suitability for gas–liquid and liquid–liquid equilibrium prediction [45]. Alternatively, PC-SAFT has shown strong predictive capabilities for gas solubility and is sometimes employed for ILs-based separation or reactive systems [46–48]. For reactive operations such as CO_2 absorption or reactive distillation, reactions can be defined using the React-Dist formalism in Aspen Plus®, allowing kinetic or equilibrium modeling within RADFRAC columns [49–51]. For detailed guidance on implementing ILs in Aspen Plus ®, the methodology described by [52] provides a comprehensive reference.

The Aspen–Python for Carbon Capture (AsPyCC) framework is organized into four modular stages: (a) absorber design, (b) heat exchanger and stripper design, (c) cross-heat exchanger integration, and (d) recycle-loading correction. A detailed description of the scheme is presented below.

(a) Absorber design

The framework begins by initializing an Aspen Plus® document containing a RadFrac block, along with the required process streams: flue gas, clean gas, lean NH_3, and rich solvent. This setup is established via the COM interface, which enables Python to programmatically define the flue gas specifications and lean solvent properties for simulation input. The absorber is designed using the infinite height column approximation [29], in which the initial column height is set to 100 m and the diameter to 12 m. The starting solvent flowrate is estimated based on a typical solvent-to-flue gas flowrate ratio, ranging from 2 to 3.5. Once the specified CO_2 capture rate (CCR) is reached by adjusting the solvent flowrate, the minimum required flowrate is identified and scaled by a factor of 1.1 to determine the effective operating value.

Subsequently, the absorber height is iteratively adjusted to match the CCR target. The column diameter is then varied, with corresponding adjustments to the solvent flowrate, to achieve the desired flooding percentage while maintaining CCR performance. A final height adjustment ensures correction of any remaining CCR deviation. These design steps, typically performed manually through trial-and-error and solver parameter refinement, are systematically automated within the proposed framework. Using the proposed approach shown in Scheme 1, the column design is automated to meet industry standards, with exogenous degrees of freedom related to the flue gas composition and flowrate. Further implementation details, including how to establish the Python–Aspen Plus® COM connection, handles convergence errors, and accesses internal Aspen Plus® variables (e.g., feed stream specifications, absorber configuration, and simulation outputs), are provided in Tables S1–S4.

(b) Heat exchanger and stripper design

In this stage of the framework, the heat exchanger, stripper, and condenser blocks are programmatically created in Aspen Plus® using the elements protocol, along with the associated process streams: *To stripper*, *Vapor*, *Reflux*, *Lean solvent*, and *CO_2*. These components are defined following the same COM-based protocol established in the absorber design stage. The initial boil-up ratio for the stripper is set between 0.01 and 0.05 to promote convergence during simulation.

To maintain geometric consistency, the height-to-diameter ratio derived from the absorber is applied to the stripper, while the diameter is determined using the same flooding-based criteria. The boil-up ratio is further refined in a subsequent step of the framework to ensure both thermal and hydraulic performance. The inputs and outputs used to modify and control Aspen Plus® from Python in this stage are summarized in Table S5 and S6. A detailed description of the procedure is provided in Scheme 2.

(c) Cross-Heat exchanger integration

Simultaneously, the *Lean solvent* stream is designated as the hot feed. The *Hot rich* and *Cold lean* streams serve as the cold and hot outlets, respectively.

This automated reconfiguration step allows for flexible energy integration strategies within the PCC process. The specific inputs and outputs used to carry out these modifications are summarized in Table S7. A detailed step-by-step description of the implementation is provided in Scheme 3.

Algorithm 3. AsPyCC: Cross-heat exchanger integration

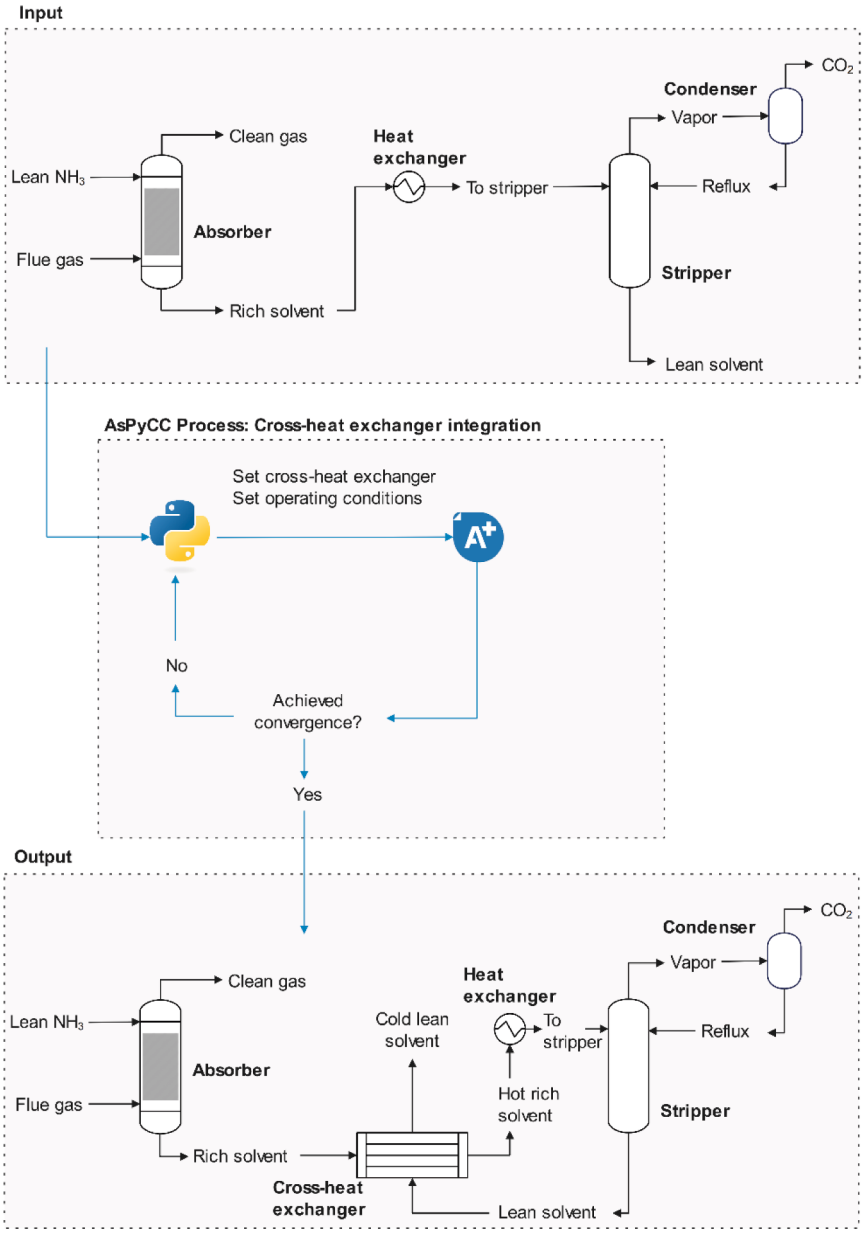

In this stage, a cross-heat exchanger is introduced using the *MHXT* block, along with the associated streams *Hot rich* and *Cold lean*. The integration is carried out using the elements protocol, which enables Python to disconnect the *Rich solvent* stream from the original heat exchanger and reassign it to the cross-heat exchanger as the cold feed.

(d) Recycle-Loading correction

In the final stage of the framework, a *Mixer* block is used to combine the *Make-up* stream with the *Cold lean* stream. The *Make-up* stream is generated using the elements protocol, with its temperature and pressure set to match those of the lean solvent. Its flowrate is computed

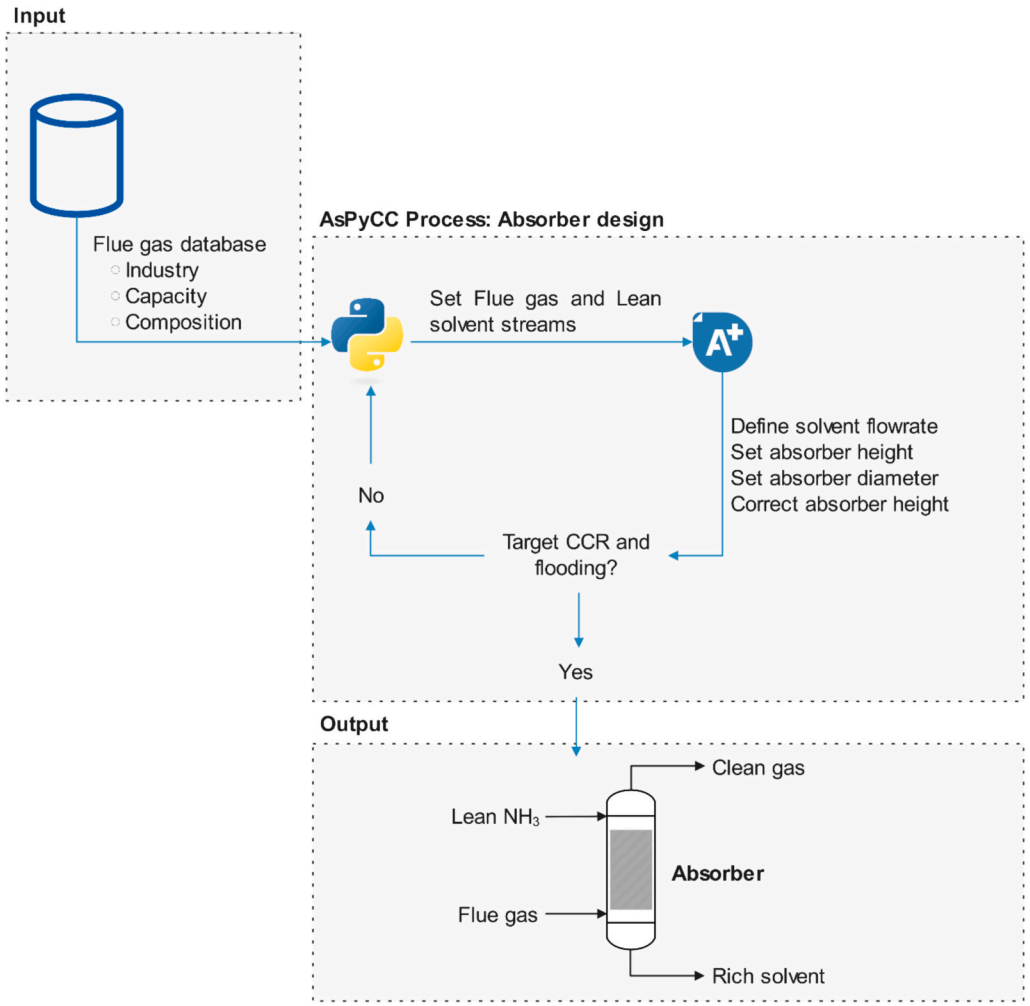

Scheme 1. AsPyCC: Absorber design.

based on the estimated NH_3 losses in the *Clean gas* and *CO_2* streams. The combined stream is then passed through a *Cooler* block to adjust its temperature, and the outlet of this block forms the *Recycle* stream.

The CO_2 loading of the *Recycle* stream is calculated as the ratio of the apparent CO_2 mole composition to the apparent NH_3 mole composition. The apparent CO_2 composition includes contributions from NH_2COO^-, HCO_3^-, CO_3^{2-}, and undissolved CO_2, while the apparent NH_3 composition includes NH^{4+}, NH_2COO^-, and undissolved NH_3. If the calculated loading exceeds the specified target value of 0.12, the boil-up ratio is increased; otherwise, it is decreased.

Finally, a 1 % purge is introduced before the *Lean NH_3* stream, which is designated as the tear stream in the simulation. The tear stream solver is configured using the Broyden algorithm with a tolerance of 1×10^{-5}, as recommended by [53]. The loop is closed by replacing the *Recycle* stream with the original *Lean NH_3* stream, and the simulation is executed one final time to extract the results. The specific inputs and outputs involved in this stage are summarized in Table S8. A simplified representation is provided in Scheme 4.

2.3. Case study: Techno-economic evaluation of PCC units

The techno-economic evaluation presented in this work assesses the performance of PCC across different industries and plant capacities. The analysis aims to evaluate the CO_2 capture potential of the selected industrial sectors, focusing on the following key performance indicators (KPIs):

- *CO_2 product flowrate (t/h)*: The amount of CO_2 removed from the flue gas stream, leaving the process after the stripping section for storage or utilization.
- *Reboiler duty (MW)*: The heat required in the stripper reboiler for solvent regeneration.
- *Regeneration energy (kJ/kg_{CO2})*: The energy consumption per unit of CO_2 captured in the PCC unit.
- *CAPEX (MUSD)*: The total capital investment required for equipment procurement, engineering, installation, and construction.
- *OPEX (MUSD/year)*: The annual operating costs, including materials and utilities.
- *Carbon capture cost ($/$t_{CO2}$)*: The ratio of annual operational costs to the amount of CO_2 captured.
- *NH_3 loss (wt.%)*: The percentage of NH_3 lost in the clean gas stream relative to the solvent provided in the lean solvent.

Additionally, to ensure a feasible design, the absorber height and diameter are included in the analysis.

2.3.1. Flue gas data generation

Flue gas compositions and flow rates were generated using the Sobol sequence within data ranges representative of various industrial sectors, as summarized in Table 4. The Sobol sequence is a widely used quasi-random, low-discrepancy method for generating uniform parameter samples [54], with further details available in [55]. The proposed data generation algorithm is outlined in Algorithm 1. In this approach, composition ranges for different industrial sectors are input into the

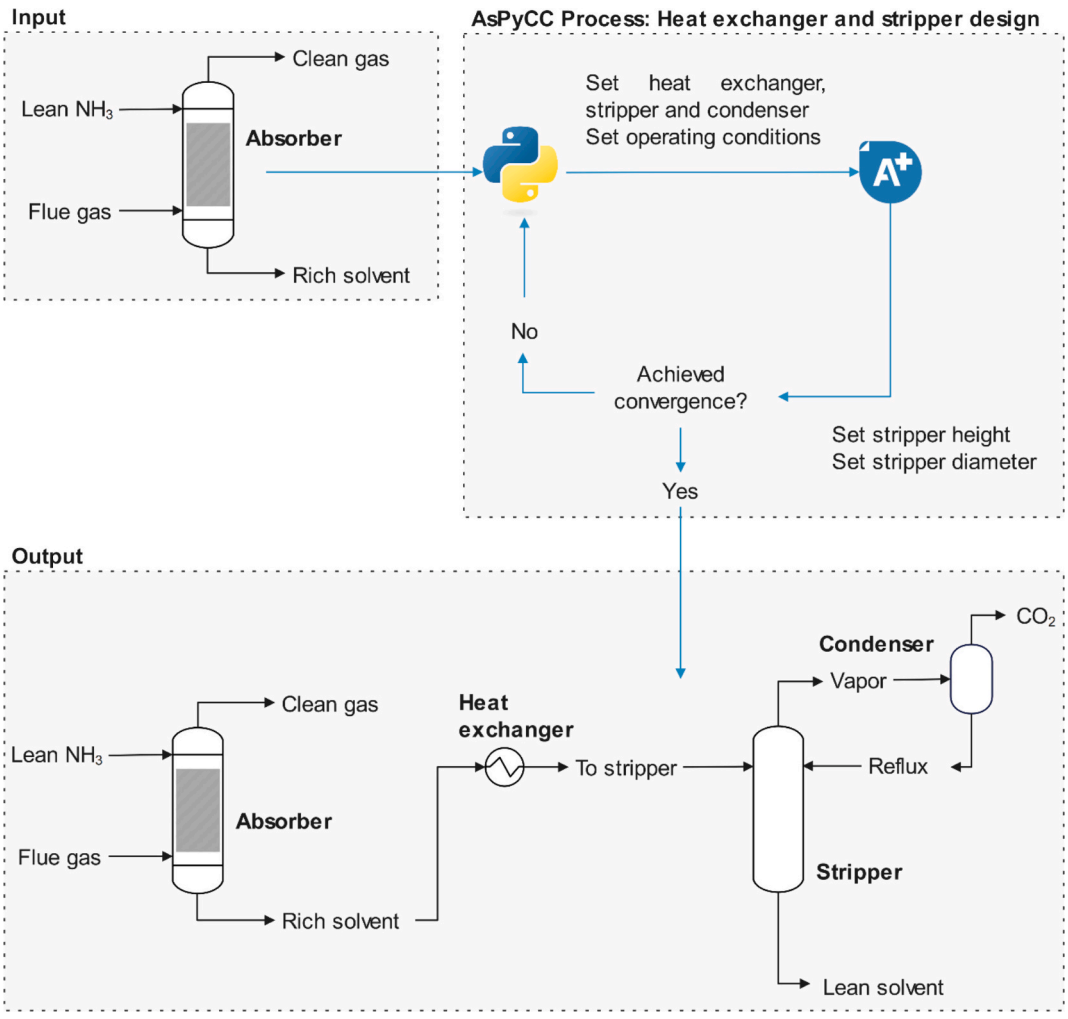

Scheme 2. AsPyCC: Heat exchanger and stripper design.

Sobol sequence, where percentage compositions are converted to mass fractions while ensuring their sum equals one.

The number of samples was determined based on the combination of five representative plant capacities (100–500 t/h) and seven industrial sectors, resulting in 35 distinct PCC configurations. The sample size was chosen so that every relevant sector–capacity combination was included at least once. Within each configuration, operating and flue gas parameters were generated using the Sobol low-discrepancy sequence, which provides a more uniform and space-filling distribution than purely random sampling [56]. This approach ensures a diverse yet representative coverage of the multidimensional input space, capturing realistic variations in flue gas compositions across different industrial sources while maintaining computational tractability.

A total of seven industrial sectors were analyzed: Cement, Coal-Fired Power Plant (CFPP), Natural Gas-Fired Power Plant (NGFPP), Gas Turbine Power Plant (GTPP), Steel, Pulp and Paper (PaP), and Fluid Catalytic Cracking (FCC). The number of variables corresponds to the typical species present in flue gas, while their labels represent the respective gas components. The minimum and maximum percentage values define the composition bounds for sampling. PCC unit capacities varied between 100 and 500 t/h.

Algorithm 1 Flue gas sample generation

Input: Flue gas composition ranges database:$FG_{data} = [Industry, Species, Ranges]$
Number of samples (N)

for *Industry* in FG_{data}:
  Define number of model inputs:$D = len(Species)$
  Define problem:$p(D, Species, Ranges)$
  Generate samples:$s(p, N)$
  if $sum(s_i) \neq 1$ with $i = 1, ..., N$:
    Regenerate samples
      if $sum(s_i) \neq 1$ persist after regenerating, ***discard*** s_i
  else:
    Scale samples:$s_i / sum(s)$
    return flue gas composition data:$FGC_{data} = [Industry, Species, Scalesamples]$
for *Industry* in FGC_{data}:
  Define flowrate range:$Flowrate_{range} = [100, 200, 300, 400, 500]$
  for *F lowrate* in $Flowrate_{range}$:
    assign $random(Scalesamples)$ to *Flowrate*
    return $Samples_{database} = [Industry, Species, Scalesamples, Flowrate]$

Output:
Flue gas composition and flowrate data base ($Samples_{database}$)

2.3.2. Ammonia cost sensitivity analysis

A sensitivity analysis was conducted to evaluate the impact of

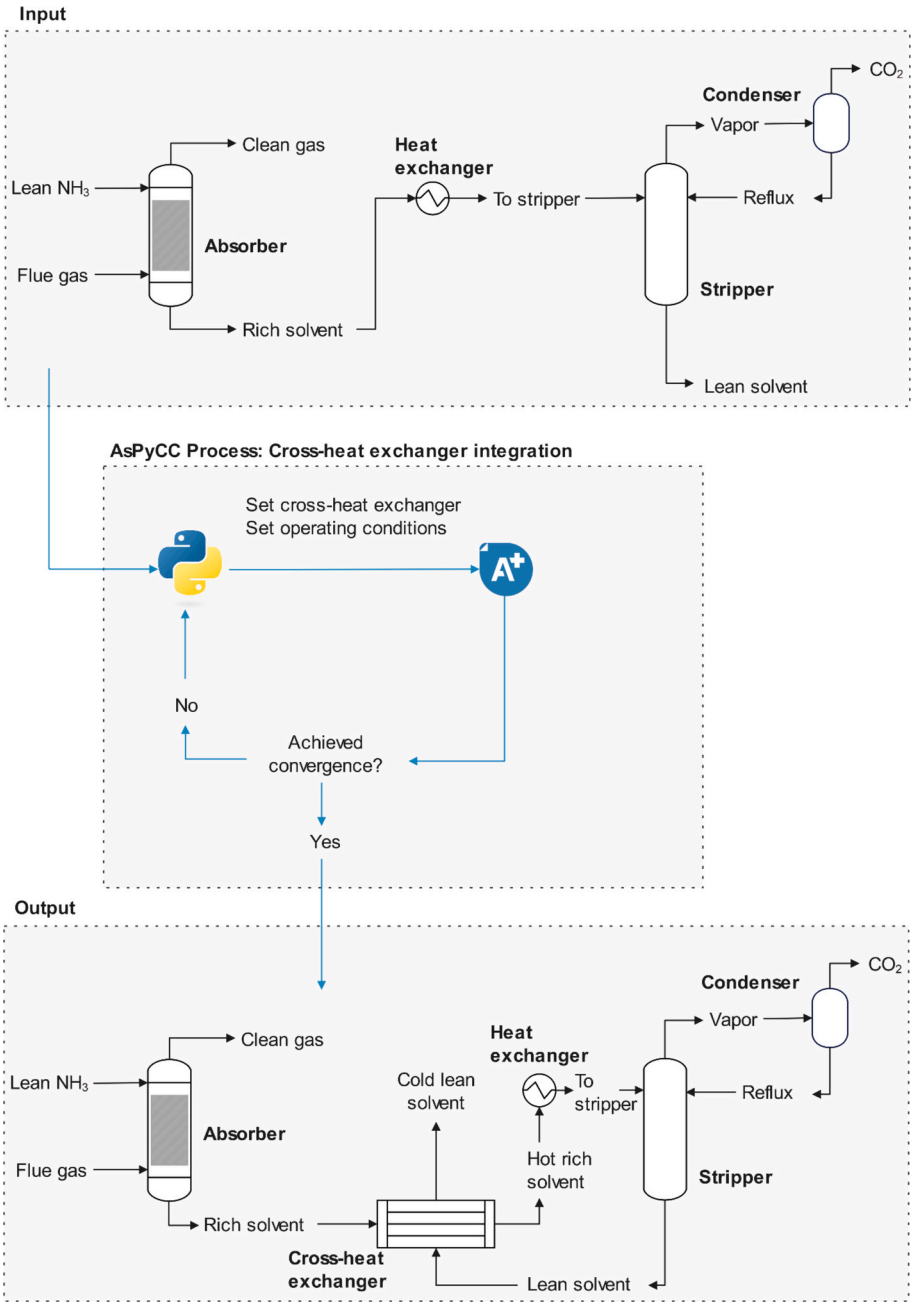

Scheme 3. AsPyCC: Cross-heat exchanger integration.

ammonia production costs on OPEX and overall carbon capture cost across all process scenarios. The cost of ammonia was adopted from the work of [70] where three representative production pathways were analyzed: Methane-to-Ammonia (MtA), Biomass-to-Ammonia (BtA), and Power-to-Ammonia (PtA). Each pathway reflects a different energy source and technological maturity:

- MtA represents the conventional natural-gas-based Haber–Bosch process, offering the lowest production cost but highest fossil dependence.
- BtA captures renewable routes using biomass-derived hydrogen, typically with intermediate costs and carbon footprints.
- PtA represents the fully renewable electricity-driven synthesis of ammonia via water electrolysis, with costs highly dependent on electricity prices.

For each pathway, the reference study reported several scenarios (e.g., maximum efficiency, minimum cost, and electricity price variations), yielding production costs ranging from $35 to $666 per ton of NH_3 as shown in Table 5. These values were integrated into the AsPyCC framework by multiplying the reported ammonia makeup flowrate by each unit cost, resulting in a set of updated OPEX and total carbon capture costs. This approach enabled a comprehensive evaluation of how ammonia price variability propagates through the economics of PCC systems across different industries and plant scales.

2.3.3. *Evaluation of PCC units*

The KPIs outlined above, along with additional carbon capture-related parameters, were selected to evaluate trade-offs between capture efficiency, economic feasibility, and process design constraints. These parameters included CCR, CO_2 production, reboiler duty, regeneration energy, CAPEX, OPEX, CO_2 capture cost, available CO_2, absorber

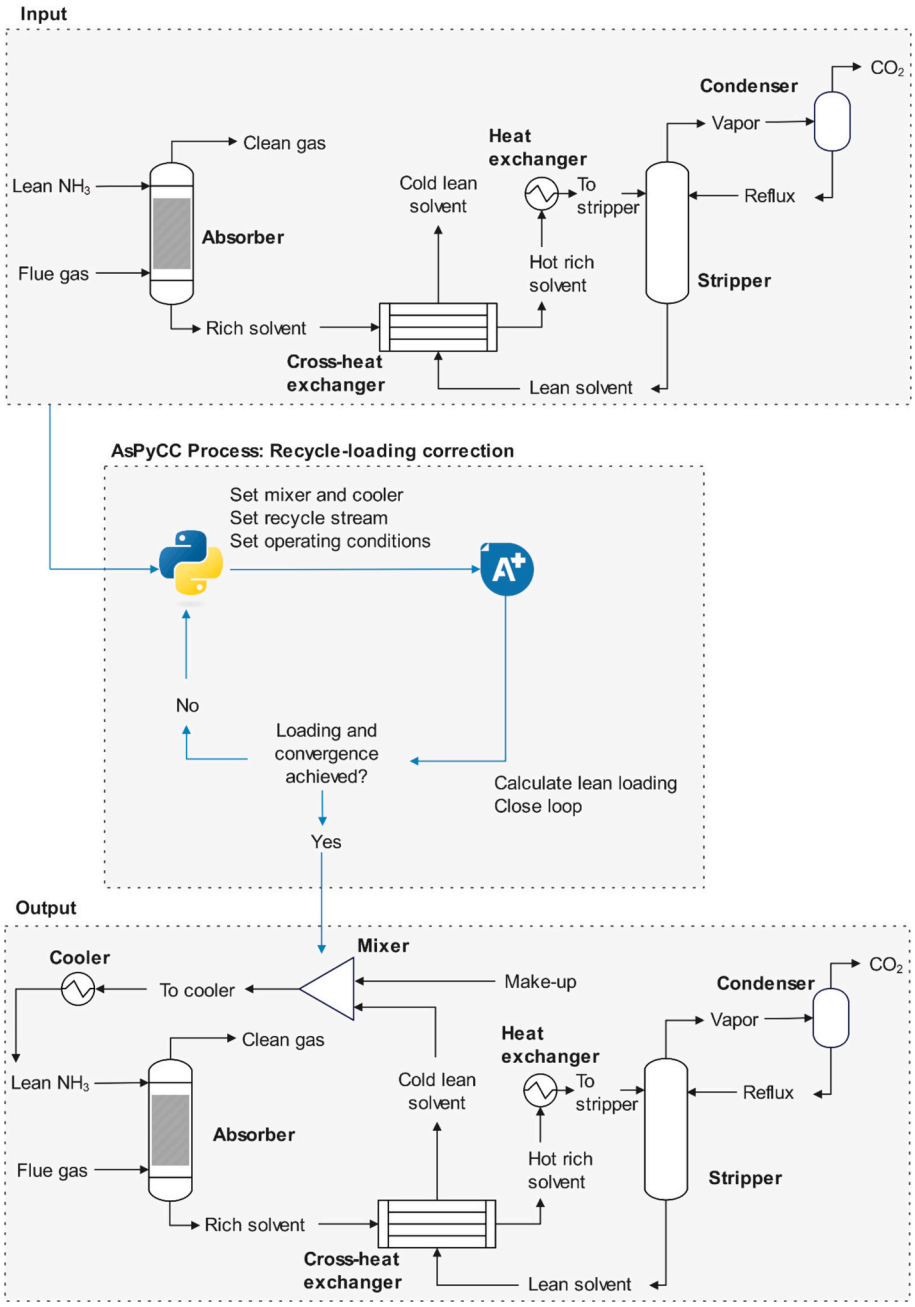

Scheme 4. AsPyCC: Recycle-loading correction.

Table 4
Flue gas composition ranges for different industrial sectors.

Industry sector	Species [wt.%]						Source
	N_2	O_2	CO_2	CO	H_2	H_2O	
Cement	[57–68]	[2–10]	[11–28]	N/A	N/A	[1.18–18.2]	[57,58]
CFPP	[65–77]	[3–5]	[10–14]	N/A	N/A	[8–10]	[59,60]
NGFPP	[70,71]	[2.4–13]	[8.6–9]	N/A	N/A	[7.8–17.3]	[59,61]
GTPP	[74.4–75.7]	[12.6–13.8]	[3.4–3.8]	N/A	N/A	[6.9–8.3]	[61–63]
Steel	[50–68]	N/A	[17–28.5]	[20–22]	[1–5]	[3.8–10]	[64–66]
PaP	[47.4–67.6]	[1.2–2.3]	[13–20.4]	N/A	N/A	[17–30.9]	[64,67]
FCC	[72–78]	[1–3]	[13–18]	N/A	N/A	[3.6–10]	[68,69]

height-to-diameter ratio (H/D), solvent-to-feed ratio (S/F), and NH_3 loss. To ensure uniform weighting across variables, the data was standardized to eliminate scale disparities.

K-means clustering was applied to classify industries based on their carbon capture characteristics. The optimal number of clusters was determined using the elbow method, which assesses the within-cluster sum of squared errors as a function of cluster count. The point at which additional clusters yielded minimal variance reduction was

selected as the optimal cluster number [71]. Following clustering, mean feature values for each cluster were computed to assess performance. To facilitate comparison, feature values were normalized, ensuring all variables were evaluated on a common scale. A multi-criteria scoring function was developed, prioritizing high CCR and CO_2 production while minimizing CAPEX, OPEX, and NH_3 loss to reflect both process efficiency and economic feasibility. The computed cluster scores were ranked, with the highest-ranked cluster representing the optimal balance between capture efficiency, cost-effectiveness, and operational feasibility.

Within the best performing cluster, PCC cases were scored based on the following indicators:

- Industry Score Index (ISI): The ratio of cases from a specific industry within the cluster to the total number of cases in the initial dataset.
- Capacity Score Index (CSI): The ratio of cases from a specific capacity within the cluster to the total number of cases in the cluster.
- Available CO_2 Score Index (ACSI): The ratio of the higher amount of CO_2 available for capture in the cluster to the amount of CO_2 entering a specific scenario.

3. Results and discussion

3.1. AsPyCC performance

The AsPyCC framework was executed on a system equipped with an AMD Ryzen 5 5500 CPU, using Aspen Plus® V14 and Python 3.13. The average computational time required to design and simulate a single PCC unit was approximately 9.30 min. Within this total, the absorber design stage accounted for the majority of the computational effort (90.10 %), followed by the recycle-loading correction (3.10 %), heat exchanger and stripper design (1.70 %), and cross-heat exchanger integration (0.80 %). The remaining 4.30 % was attributed to algorithm initialization steps, including library imports, data loading, and simulation file preparation. An Aspen Plus flowsheet is shown in Fig. S1 in the supplementary information.

The absorber design module accounts for around 90 % of total computational time due to three sequential iterative subroutines: determination of the minimum solvent flowrate, effective capture height, and column diameter, each requiring full convergence of Aspen Plus® before proceeding. The sequential dependency limits opportunities for parallelization, although dividing variable ranges among multiple Aspen Plus ® instances could offer efficiency gains. The average computation time for this stage is around 9 min, and further reduction is not considered critical at this stage of the AsPyCC framework.

The comparatively high computational cost of the absorber stage arises from the need to simultaneously satisfy two performance targets: achieving the specified CO_2 capture rate and maintaining an acceptable flooding percentage. In contrast, the subsequent stages of the framework primarily require numerical convergence, resulting in significantly lower computational loads.

The framework demonstrated a high level of robustness, with a success rate of approximately eight absorber design completions for every failed attempt, the latter primarily due to COM interface or Aspen Plus® execution errors. All other components of the AsPyCC framework completed successfully without errors across all simulations.

COM connection errors occur when the established link between Python and Aspen Plus® is disrupted. Several factors can contribute to this issue, including executing the code before Aspen Plus® has completed its calculations, improper loading of the simulator modules, or interference from external applications. Within the AsPyCC framework, the most common cause of COM errors is related to the state of Aspen Plus®, for instance, when operating conditions are specified, the framework may attempt to execute the simulation before the software has fully processed the changes. The likelihood of encountering this error depends on the hardware being used, with faster CPUs handling simulations more efficiently, while slower systems are more susceptible to processing delays.

Although limited information is available in the literature regarding Python-Aspen Plus® errors, the development of the AsPyCC framework provides an opportunity to explore these issues and implement strategies for prevention and handling of errors. For *AttributeError* occurrences, the *try-except* statement in Python can be used to catch these errors, allowing the simulation to be reinitialized or re-dispatched [72]. Similarly, COM errors can be handled using the same approach; however, these methods may lead to increased computational time. These strategies will be incorporated into future versions of the framework to enhance its robustness. Since Aspen Plus® is a closed-source simulator, error causes such as memory overflow or division by zero are inaccessible, making universal prevention strategies difficult to achieve. Nonetheless, the adopted error-handling approach ensures robust execution across all 35 scenarios. Overall, the AsPyCC framework enables the efficient design of PCC units within a relatively short time, facilitating the evaluation of various decarbonization scenarios.

3.2. Designed PCC units

A total of 35 PCC units were designed using the AsPyCC framework and evaluated based on the KPIs defined in the Methodology section. The average CCR across all designed units was 89.70 %, primarily influenced by the CCR of GTPP units, which averaged 87.12 %. Excluding GTPP units, the remaining units achieved an average CCR of 90.01 %, demonstrating effective CO_2 capture performance consistent with values reported in the literature [15,73,74].

GTPP units exhibited the highest NH_3 loss, averaging 23 % of the initial loading, equivalent to 33700 ppm, which exceeds the reported maximum of 19000 ppm in the literature. The low CO_2 content in the flue gas makes the formation of ammonium bicarbonate unfavorable, leaving free NH_3 in the solution. Moreover, at lower total pressures, corresponding to lower CO_2 concentrations, the partial pressure of NH_3

Table 5
NH_3 cost based on production pathway.

Production pathway	NH_3 cost [$/t]
MtA MEP*	387
MtA MCP**	374
BtA MEP	505
BtA MCP	450
PtA MEP	666
PtA MCP	544
PtA A***	482
PtA B***	453
PtA C***	281
PtA D***	35

*MEP: Maximum efficiency point
**MCP: Minimum cost point
***A: 1060 $/stack, B: 470 $/stack, C: 35 $/MWh, D: 0 $/MWh

Table 6
Summary of principal averaged PCC KPIs for the selected industry sectors.

Industry	KPI CCR [%]	Reg. energy [kJ/kg_{CO2}]	CAPEX [MUSD]	OPEX [MUSD/year]	Carbon capture cost [$/$t_{CO2}$]	NH_3 loss [%]
Cement	90.01	2906.13	22.68	18.93	45.46	4.30
CFPP	90.00	3050.47	20.84	15.14	51.48	6.30
NGFPP	90.00	3212.19	19.31	11.82	59.69	8.31
GTPP	87.12	3016.23	16.05	14.39	173.76	23.00
Steel	90.04	2867.58	36.38	42.83	96.08	5.81
PaP	90.01	2837.75	29.92	37.83	103.37	4.24
FCC	90.00	2895.25	30.45	36.60	103.67	5.57

in the vapor phase increases, further enhancing NH_3 losses [75,76].

The equilibrium partial pressure of NH_3 above the CO_2-lean solution increases with temperature and with the amount of free (unreacted) NH_3 in the solvent; conversely, increased CO_2 partial pressure (or higher CO_2-loading) promotes formation of ammonium bicarbonate/carbonate species, reducing free NH_3 activity and vapor pressure [41,77,78]. In our GTPP cases the available CO_2 for capture is comparatively low (3.48–17.41 t/h), and the solvent-to-flue gas ratio is relatively close (1.5–1.7), while the simulations use a fixed lean loading of 0.12 at an absorber temperature of 50 °C. The combination of limited CO_2 availability, the fixed low loading (i.e., greater NH_3 excess relative to CO_2), and the elevated absorber temperature leads to higher equilibrium NH_3 partial pressures and thus higher NH_3 slip [79].

In contrast, all other units maintained NH_3 loss below 10 %, within the reported range of 4500–19000 ppm [41]. The regeneration energy requirements for all cases fell within the reported range of 1000–4200 kJ/kg_{CO2} [13].

Regarding CAPEX and OPEX, both increased with plant capacity. However, at 100 t/h, the absorber height was the tallest while the diameter was the smallest. This is attributed to the small amount of solvent required based on the flue gas-to-lean solvent ratio, requiring a tall and narrow column to achieve 90 % CCR while maintaining a flooding range of 70–80 % [80]. Finally, the carbon capture cost ranged from 43.74 $/t_{CO2}$ to 252.83 $/t_{CO2}$. With the carbon price currently ranging from 35 $/t_{CO2}$ to 250 $/t_{CO2}$ [81–87], the resulting values in the same order of magnitude indicate that integrating a PCC unit into an existing industrial plant is technically and economically feasible. It is worth noting that CO_2 compression costs were not included in this analysis, as the design of the compression train depends on the specific CO_2 conditions required for further chemical upgrading or sequestration. A summary of the PCC units designed by the AsPyCC framework is shown in Table 6.

3.3. Sensitivity analysis

The sensitivity analysis revealed clear trends in how NH_3 production pathways and plant capacities affect the overall carbon capture cost. Across all sectors, accounting for ammonia sourcing increased capture costs by 1.70–609.65 %, depending on the production route. MtA pathways consistently resulted in the lowest cost increments, reflecting their lower ammonia production cost, whereas PtA pathways, particularly under high electricity price conditions, produced the largest increases in total OPEX and carbon capture cost.

The lowest relative increase in carbon capture cost across all scenarios occurred in the PaP scenario at 200 t/h under the PtA-D pathway, with only a 1.63 % increment, despite showing an NH_3 loss of 3.45 %. In contrast, the cement plant scenario at the same capacity and a comparable CCR (90.06 %) exhibited a 36.96 % increase under identical NH_3 pricing conditions. This discrepancy stems from the interplay between solvent makeup rate, baseline OPEX, and sector-specific process characteristics. The PaP case exhibited a lower solvent makeup requirement (1.62 t/h vs. 2.03 t/h), directly reducing NH_3 replacement costs. Moreover, its higher base OPEX (27.75 MUSD/year) diluted the impact of added NH_3 costs in relative terms. Conversely, the cement plant, with its lower baseline OPEX and higher solvent consumption per unit CO_2 captured, showed amplified sensitivity to NH_3 price fluctuations.

Although the 100 t/h GTPP scenario exhibits a slightly higher NH_3 loss percentage (27.3 % vs. 24.5 %), the 200 t/h GTPP case produces a much larger relative increase in carbon capture cost (+609.6 % vs. + 275.7 %). In the 200 t/h GTPP case the make-up is substantially higher (3.88 t/h vs. 2.13 t/h), so the absolute annual cost of NH_3 replacement under the PtA MEP price is much larger. At the same time the 200 t/h case has a lower baseline OPEX (4.75 MUSD/yr) and only a modest increase in CO_2 throughput (5.80 t/h), so the added NH_3 expense represents a large fraction of operating costs and, when divided by a small CO_2 captured flow, yields a very high carbon capture cost increment. By contrast, the 100 t/h case, despite its higher fractional NH_3 loss, has lower absolute NH_3 consumption and a higher baseline OPEX (6.20 MUSD/yr), which attenuates the relative impact of NH_3 cost.

When analyzed by industry, cement and CFPP scenarios exhibited the most moderate cost increases, averaging 92.75 $/t_{CO2}$ and 120.34 $/t_{CO2}$, respectively, due to their relatively low specific NH_3 consumption per ton of CO_2 captured. In contrast, GTPP and FCC sectors were more sensitive, reaching 546.32 $/t_{CO2}$ and 173.34 $/t_{CO2}$, respectively, driven by higher solvent makeup rates. Regarding plant scale, larger capacities (400–500 t/h) tended to mitigate the effect of NH_3 price

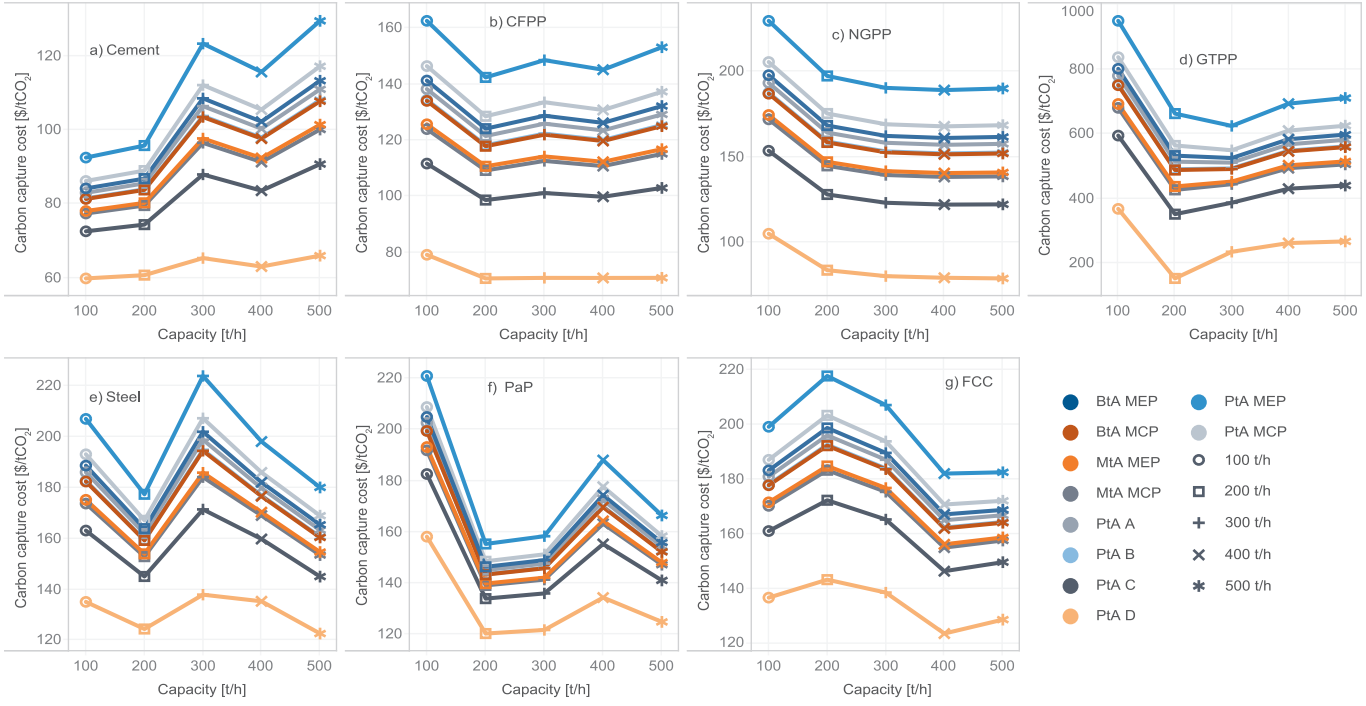

Fig. 2. Carbon capture cost sensitivity analysis based on different ammonia production pathways.

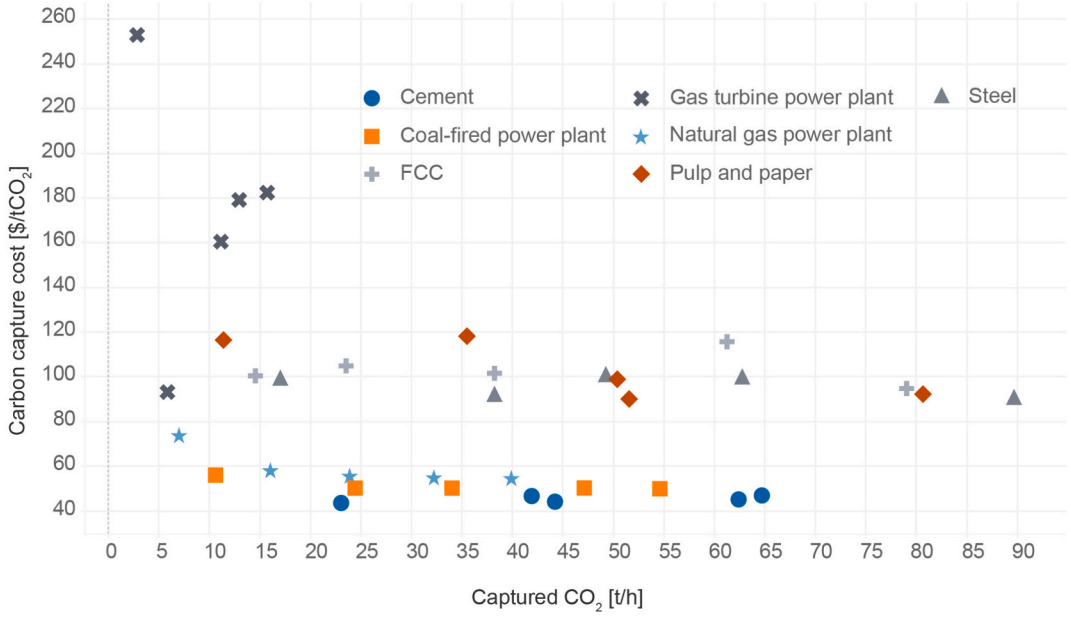

Fig. 3. Scatter plot of Carbon capture cost vs captured CO_2.

Table 7
Summary of principal PCC KPIs for the selected industry sectors.

Cluster	KPI CCR [%]	Reg. energy [kJ/ kg_{CO2}]	CAPEX [MUSD]	OPEX [MUSD/ year]	Carbon capture cost [$/$kg_{CO2}$]	NH3 loss [%]
0	85.98	2951.80	14.22	11.78	135.15	15.85
1	89.79	2992.75	23.40	22.68	69.45	5.73
2	90.05	2902.83	51.68	61.05	98.55	4.84

fluctuations, as fixed operating costs were distributed over a greater CO_2 capture throughput. Conversely, smaller units (100–200 t/h) displayed higher volatility in capture costs, underscoring the influence of process scale on economic resilience.

Overall, including NH_3 production cost shifted total carbon capture costs from approximately 44–250 $/$t_{CO2}$ (base OPEX) to 60–950 $/$t_{CO2}$ under the most expensive PtA scenarios. Despite this increase, most cases remain within the same order of magnitude as current carbon

Table 8
Normalized scoring metric for the defined lusters.

Cluster	KPI CCR [%]	Reg. energy [kJ/ kg_{CO2}]	CAPEX [MUSD]	OPEX [MUSD/ year]	Carbon capture cost [$/$kg_{CO2}$]	NH3 loss [%]
0	0.94	1.00	0.24	0.22	0.00	0.08
1	1.00	0.00	1.00	1.00	0.44	0.00
2	0.00	0.55	0.00	0.00	1.00	1.00

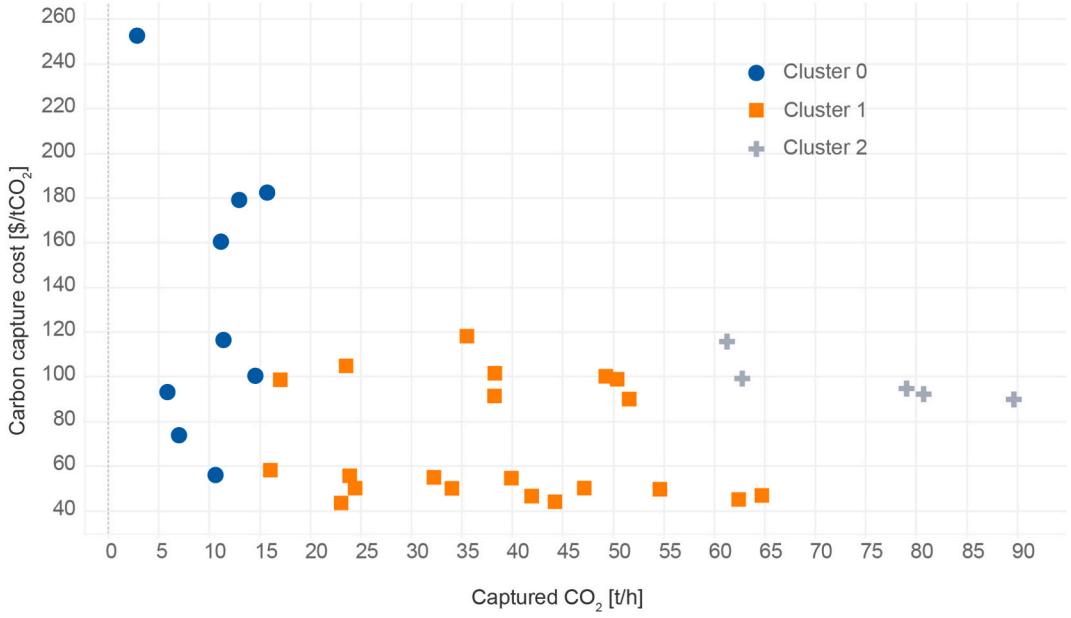

Fig. 4. Scatter plot of Carbon capture cost vs captured CO_2 based on clusters.

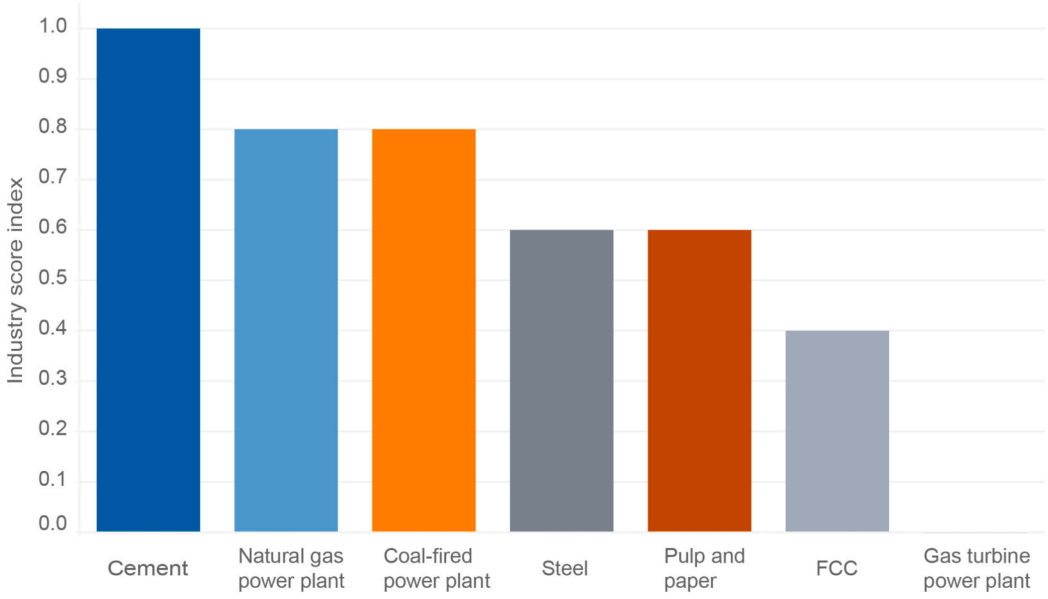

Fig. 5. Industry score index (ISI) for the industry in best performing cluster.

Table 9
Capacity score index for the capacities in best performing cluster.

Capacity [t/h]	100	200	300	400	500
Capacity score index (CSI)	0.10	0.30	0.30	0.19	0.14

Table 10
Available CO_2 score index (ACSI) for best performing capacity.

Industry	Capacity [t/h]				
	100	200	300	400	500
Cement	0.36	0.44	0.65	0.96	1.00
CFPP	0.00	0.38	0.53	0.73	0.84
NGFPP	0.00	0.25	0.37	0.50	0.62
GTPP	0.26	0.59	0.76	0.00	0.00
Steel	0.00	0.55	0.80	0.78	0.00
PaP	0.00	0.36	0.59	0.00	0.00
FCC	0.36	0.44	0.65	0.96	1.00

market prices, suggesting that integrating renewable or hybrid ammonia supply chains can remain economically competitive across most industrial sectors analyzed. Scenarios exceeding the upper range of carbon market prices were classified as economically infeasible, as discussed in Section 3.4. Results from the sensitivity analysis are presented in Fig. 2.

3.4. Feasible CC units

To better assess the selection of optimal conditions for carbon capture, principal component analysis (PCA) and clustering were performed. A plot of carbon capture cost versus captured CO_2 is shown in Fig. 3. It can be observed that certain industry sectors fall within a region where the carbon capture cost is relatively low. To identify the characteristics that led these scenarios to fall within this region and to define its boundaries as suitable for carbon capture, a cluster analysis was performed.

A clustering analysis was conducted to classify industrial carbon capture cases based on key performance indicators, including CCR, reboiler duty, regeneration energy, capital and operational expenditures, and NH_3 loss. The dataset was standardized using z-score normalization, ensuring comparability across variables by adjusting for differences in scale [88]. PCA was employed to capture patterns of similarity among observations by reducing dimensionality while preserving variance [89]. The optimal number of clusters was determined using the Elbow Method, which identified three clusters as the most suitable grouping.

The PCA scores suggest that the different scenarios can be grouped based on the selected features, with the contributions of CCR, regeneration energy, CAPEX, OPEX, and NH_3 loss to the principal components outlined in Table 7. The scenarios from different industries were mapped based on these scores, as shown in Fig. 4. Each cluster was characterized using the mean values of the selected features, revealing key trends in performance. Clusters 1 and 2 demonstrate effective CCR values; however, Cluster 2 has higher CAPEX, OPEX, and carbon capture costs, although it achieves a higher CCR and lower NH_3 loss compared to Cluster 1. On the other hand, Cluster 0 exhibits the lowest CAPEX and OPEX but underperforms in terms of CCR, achieving the highest carbon capture cost of all three clusters. This suggests that while Cluster 0 may offer cost savings in terms of capital and operational expenditures, its lower efficiency in carbon capture results in higher overall costs.

To determine the most favorable cluster for carbon capture applications, a scoring metric based on normalized means was developed, prioritizing higher CCR and CO_2 production while penalizing higher CAPEX, OPEX, and NH_3 loss. The comparison of normalized cluster means revealed that Cluster 1 achieved the highest score, indicating that it represents the most economically and technically viable set of industrial cases. The performance of the clusters is summarized in Table 8. The PCA visualization (Fig. 4) further demonstrates distinct separations between clusters, highlighting inherent differences in economic and operational characteristics. To refine the selection of the most suitable region for carbon capture, the ISI, CSI, and ASCI metrics were analyzed. For the ISI metric (Fig. 5), the cement plant emerged as the most suitable scenario, with a score of 1. In contrast, natural gas and coal-fired power plants scored 0.8, demonstrating their relative suitability for PCC. Steel and pulp and paper industries scored 0.6, followed by FCC with a score of 0.4, while gas turbine power plants scored 0, indicating the least suitability for PCC.

The CSI metric favored the 300 t/h plant capacity for PCC with a score of 0.3, the same as the 200 t/h capacity, as shown in Table 9. This suggests that these capacities provide sufficient CO_2 entering the PCC unit, resulting in higher solvent flowrates and more feasible column dimensions, ensuring hydraulic soundness. Larger capacities require taller columns, increasing the economic investment. The 100 t/h

Table 11
Process design parameters of selected feasible PCC units.

Case	CO2 concentration [wt.%]	S/F ratio	NH3 make-up [t/h]	Absorber height [m]	Absorber diameter [m]	Stripper height [m]	Stripper diameter [m]	Regeneration energy [kJ/kgCO2]
Cement-200	24.52	6.29	2.03	20.7	6.5	11.58	3.63	2897.66
Cement-300	15.50	4.23	3.18	25.5	7.25	14.26	4.05	2955.03
CFPP-200	13.54	3.812	2.28	26.2	6.1	14.65	3.41	2965.55
CFPP-300	12.58	3.68	3.45	26.9	7.2	15.04	4.02	3087.29
NGPP-200	8.88	2.83	2.38	29.2	5.8	16.33	3.24	3159.45
NGPP-300	8.88	2.86	3.44	27.3	7.2	15.27	4.02	3249.82

capacity score was 0.1, making it the least suitable for PCC. The ACSI score analysis revealed that for a 200 t/h capacity, a CO_2 concentration range of 17–19 % is favorable, while for 300 t/h capacity, 11–17 % is optimal. For 400 t/h, a composition of 11–15 % is favorable, and for 500 t/h, a concentration range of 8–13 % is considered suitable. These ACSI scores are summarized in Table 10.

Representative process design parameters were compiled for the most viable industries identified in Cluster 1 and by the scoring metrics defined in section 2.3.3. Table 11 summarizes key design and operating variables. These data provide practical guidance for scaling and retrofitting PCC units in large stationary sources, bridging the gap between the methodological assessment and real industrial implementation.

4. Conclusions and future work

In this work, a comprehensive techno-economic evaluation of different post-combustion carbon capture (PCC) units was performed using the novel AsPyCC framework, applied to seven industrial sectors. The main objective of this study was to assess the feasibility of incorporating PCC technology into key industrial sectors, using an automated framework for design, sizing, and simulation of PCC units in Aspen Plus through Python. The AsPyCC framework successfully designed 35 units that met industry standards, with internal constraints ensuring compliance with the selected parameters of 90 % CO_2 capture rate (CCR), 0.12 ammonia (NH_3) loading, and 5 wt% NH_3 in the solvent. The designs achieved an average CCR of 89.70 %, with several sectors demonstrating NH_3 loss of less than 10 % of the initial amount, and regeneration energy requirements within the ranges reported in the literature. These results demonstrate the feasibility of utilizing PCC in diverse industrial applications.

To further assess the suitability of the design framework and the selected industrial sectors, clustering analysis was performed, supported by principal component analysis (PCA). This analysis identified three distinct clusters of industrial cases based on economic and operational characteristics. Cluster 1 emerged as the most favorable, balancing high CCR with cost-effectiveness, while Cluster 0, although cost-efficient, had a lower CCR and higher carbon capture cost. The ISI and CSI metrics helped refine the suitability of specific sectors and plant capacities, highlighting that cement plants (ISI = 1) and natural gas and coal-fired power plants (ISI = 0.8) were the most favorable for PCC, with the optimal plant capacities for PCC implementation identified as 200 t/h and 300 t/h.

Additionally, the ASCI analysis revealed the optimal CO_2 concentration ranges for each plant capacity. For 200 t/h plants, CO_2 concentrations between 17–19 % were found to be most favorable, while for 300 t/h plants, concentrations between 11–17 % were optimal. These findings suggest that while PCC is feasible across a range of industries, the most suitable conditions depend on plant type, capacity, and CO_2 concentration.

The sensitivity analysis provided deeper insight into the relative influence of key process variables on both technical and economic outcomes. Variations in parameters such as CO_2 concentration, solvent makeup flow, and ammonia loss were found to have the strongest impact on carbon capture cost and overall process feasibility. The analysis revealed that even under similar ammonia pathway conditions, differences in process scale and NH_3 recovery efficiency can significantly alter the carbon capture cost increment. This highlights the nonlinear and interdependent nature of PCC system behavior, reinforcing the need for comprehensive multi-parameter assessments during design and optimization.

Looking ahead, further enhancements to the AsPyCC algorithm will include the incorporation of additional constraints related to NH_3 loss, column height limits, and economic considerations. An optimization framework could also be added to the algorithm to design not only compliant but also optimal PCC units, maximizing both efficiency and economic feasibility. There is the opportunity to change the assumed solvent type and capture rate at the initial step of the algorithm. With this, other sectors could perform better, as those initial assumptions come from current industry practices mainly dealing with acid gases treatment and carbon captures with amines. Expanding the framework to include additional industrial sectors will improve the categorization of relevant sectors that contribute to CO_2 emissions, as well as identify sectors that can be leveraged for CO_2 production, essential for other chemical processes.

CRediT authorship contribution statement

Fernando Zea: Writing – review & editing, Writing – original draft, Visualization, Validation, Methodology, Investigation, Formal analysis, Data curation. **Christopher Varela:** Writing – review & editing, Writing – original draft, Supervision, Methodology, Conceptualization. **Kyle V. Camarda:** Writing – review & editing, Writing – original draft, Supervision, Methodology, Conceptualization.

Declaration of competing interest

The authors declare that they have no known competing financial interests or personal relationships that could have appeared to influence the work reported in this paper.

Acknowledgements

The authors gratefully acknowledge Dr. Guenther Glatz for his valuable review and constructive feedback, which contributed to the development and improvement of this work.

Appendix A. Supplementary data

Supplementary data to this article can be found online at https://doi.org/10.1016/j.fuel.2025.137896.

Data availability

Data will be made available on request.

References

[1] Im D, Jung H, Lee JH. Modeling, simulation and optimization of the rotating packed bed (RPB) absorber and stripper for MEA-based carbon capture. Comput Chem Eng 2020;143:107102. https://doi.org/10.1016/J.COMPCHEMENG.2020.107102.

[2] Madugula ACS, Jeffryes C, Henry J, Gossage J, Benson TJ. A simulation-based model studying monoethanolamine and aprotic heterocyclic anion ionic liquid (AHA-IL) mixtures for carbon capture. Comput Chem Eng 2024;183:108599. https://doi.org/10.1016/J.COMPCHEMENG.2024.108599.

[3] Cremona R, De Lena E, Conversano A, Spinelli M, Romano MC, Gatti M. Techno-economic assessment of high temperature heat pumps integrated in MEA-based post-combustion CO2 capture for cement plant. Carbon Capture Sci Technol 2025;16:100446. https://doi.org/10.1016/J.CCST.2025.100446.

[4] Akinmoladun A, Tomomewo OS. Advances and future perspectives in post-combustion carbon capture technology using chemical absorption process: a review. Carbon Capture Sci Technol 2025;16:100461. https://doi.org/10.1016/J.CCST.2025.100461.

[5] Zhao B, Su Y, Tao W, Li L, Peng Y. Post-combustion CO2 capture by aqueous ammonia: a state-of-the-art review. Int J Greenhouse Gas Control 2012;9:355–71. https://doi.org/10.1016/J.IJGGC.2012.05.006.

[6] Kittel J, Gonzalez S, Lemaire E, Raynal L. Corrosion in post-combustion CO 2 capture plants -comparisons between MEA 30% and new processes 2012:255. https://doi.org/10.34894/VQ1DJA.

[7] Dickinson J, Percy A, Puxty G, Verheyen TV. Oxidative degradation of amine absorbents in carbon capture systems – a dynamic modelling approach. Int J Greenhouse Gas Control 2016;53:391–400. https://doi.org/10.1016/J.IJGGC.2016.08.001.

[8] Jaffar MM, Rolfe A, Brandoni C, Martinez J, Snape C, Kaldis S, et al. A technical and environmental comparison of novel silica PEI adsorbent-based and conventional MEA-based CO2 capture technologies in the selected cement plant. Carbon Capture Sci Technol 2024;10:100179. https://doi.org/10.1016/J.CCST.2023.100179.

[9] Sridhar P, Kumar A, Manivannan S, Farooq S, Karimi IA. Technoeconomic evaluation of post-combustion carbon capture technologies on-board a medium range tanker. Comput Chem Eng 2024;181:108545. https://doi.org/10.1016/J.COMPCHEMENG.2023.108545.

[10] Zhang Y, Dong L, Feng D, Dong H, Li Y, Zhao Z, et al. Kinetic properties of solventing out crystallization of ammonium bicarbonate in a novel ammonia carbon capture system. Carbon Capture Sci Technol 2022;5:100077. https://doi.org/10.1016/J.CCST.2022.100077.

[11] Villeneuve K, Roizard D, Remigy JC, Iacono M, Rode S. CO2 capture by aqueous ammonia with hollow fiber membrane contactors: Gas phase reactions and performance stability. Sep Purif Technol 2018;199:189–97. https://doi.org/10.1016/J.SEPPUR.2018.01.052.

[12] MacDowell N, Florin N, Buchard A, Hallett J, Galindo A, Jackson G, et al. An overview of CO2 capture technologies. Energy Environ Sci 2010;3:1645–69. https://doi.org/10.1039/C004106H.

[13] Zea F, Tinoco D, Varela C. A techno-economic evaluation of post-combustion carbon capture using renewable ammonia with different process configurations. Case Stud Chem Environ Eng 2023;8:100502. https://doi.org/10.1016/J.CSCEE.2023.100502.

[14] Liang Z, (Henry), Rongwong W, Liu H, Fu K, Gao H, Cao F, et al. Recent progress and new developments in post-combustion carbon-capture technology with amine based solvents. Int J Greenhouse Gas Control 2015;40:26–54. https://doi.org/10.1016/J.IJGGC.2015.06.017.

[15] Jilvero H, Normann F, Andersson K, Johnsson F. The rate of CO2 absorption in ammonia-implications on absorber design. Ind Eng Chem Res 2014;53:6750–8. https://doi.org/10.1021/IE403346A/ASSET/IMAGES/LARGE/IE-2013-03346A_0008.JPEG.

[16] Liu G, Sun S, Sun H, Zhang Y, Lv J, Wang Y, et al. Integrated CO2 capture and utilisation: a promising step contributing to carbon neutrality. Carbon Capture Sci Technol 2023;7:100116. https://doi.org/10.1016/J.CCST.2023.100116.

[17] Aceituno D, Zhang X, Hao H. A comprehensive review on carbon utilization pathways in concrete from conventional to improved strategies. Carbon Capture Sci Technol 2025;16:100467. https://doi.org/10.1016/J.CCST.2025.100467.

[18] Battaglia P, Buffo G, Ferrero D, Santarelli M, Lanzini A. Methanol synthesis through CO2 capture and hydrogenation: thermal integration, energy performance and techno-economic assessment. J CO2 Util 2021;44:101407. https://doi.org/10.1016/J.JCOU.2020.101407.

[19] Jiang S, Sun J, Zhai S, Yu T, Sun L, Yang L, et al. Ambient CO2 capture and conversion into liquid fuel and fertilizer catalyzed by a PdAu nano-alloy. Cell Rep Phys Sci 2023;4:101248. https://doi.org/10.1016/J.XCRP.2023.101248.

[20] Varela C, Zea F, Correa O, Camarda KV. A Simulation-based Integration of Carbon Capture and utilization in a Urea Production Process. Computer Aided Chemical Engineering 2024;53:2065–70. https://doi.org/10.1016/B978-0-443-28824-1.50345-8.

[21] Sadhwani N, Adhikari S, Eden MR. Biomass Gasification using Carbon Dioxide: effect of Temperature, CO2/C Ratio, and the Study of Reactions Influencing the Process. Ind Eng Chem Res 2016;55:2883–91. https://doi.org/10.1021/ACS.IECR.5B04000/ASSET/IMAGES/LARGE/IE-2015-04000M_0009.JPEG.

[22] Anwar MN, Fayyaz A, Sohail NF, Khokhar MF, Baqar M, Yasar A, et al. CO2 utilization: Turning greenhouse gas into fuels and valuable products. J Environ Manage 2020;260:110059. https://doi.org/10.1016/J.JENVMAN.2019.110059.

[23] Jeswani HK, Zapata-Boada S, Spallina V, Azapagic A. Towards net-zero in steel production: Process simulation and environmental impacts of carbon capture, storage and utilisation of blast furnace gas. Carbon Capture Sci Technol 2025;15:100387. https://doi.org/10.1016/J.CCST.2025.100387.

[24] Zhao M, Minett AI, Harris AT. A review of techno-economic models for the retrofitting of conventional pulverised-coal power plants for post-combustion capture (PCC) of CO2. Energy Environ Sci 2012;6:25–40. https://doi.org/10.1039/C2EE22890D.

[25] Lucquiaud M, Gibbins J. Effective retrofitting of post-combustion CO2 capture to coal-fired power plants and insensitivity of CO2 abatement costs to base plant efficiency. Int J Greenhouse Gas Control 2011;5:427–38. https://doi.org/10.1016/J.IJGGC.2010.09.003.

[26] Koelbl BS, Wood R, van den Broek MA, Sanders MWJL, Faaij APC, van Vuuren DP. Socio-economic impacts of future electricity generation scenarios in Europe: potential costs and benefits of using CO2 Capture and Storage (CCS). Int J Greenhouse Gas Control 2015;42:471–84. https://doi.org/10.1016/J.IJGGC.2015.08.010.

[27] Heyes A, Urban B. The economic evaluation of the benefits and costs of carbon capture and storage. Int J Risk Assess Manag 2019;22:324–41. https://doi.org/10.1504/IJRAM.2019.103337.

[28] Lee H, Lee J, Koo Y. Economic impacts of carbon capture and storage on the steel industry–a hybrid energy system model incorporating technological change. Appl Energy 2022;317:119208. https://doi.org/10.1016/J.APENERGY.2022.119208.

[29] Madeddu C, Errico M, Baratti R. CO2 Capture by Reactive Absorption-Stripping 2019. https://doi.org/10.1007/978-3-030-04579-1.

[30] Symonds R, Shokrollahi M, Hughes R, Navarri P, Modler R. Systematic approach to the design, modeling, and techno-economic-environmental analysis of CO2 capture technologies as part of the National CCUS Assessment Framework (NCAF). Carbon Capture Sci Technol 2025;16:100439. https://doi.org/10.1016/J.CCST.2025.100439.

[31] Zhang M, Guo Y. Process simulations of large-scale CO2 capture in coal-fired power plants using aqueous ammonia solution. Int J Greenhouse Gas Control 2013;16:61–71. https://doi.org/10.1016/J.IJGGC.2013.03.010.

[32] Que H, Chen CC. Thermodynamic modeling of the NH 3-CO 2-H 2O system with electrolyte NRTL model. Ind Eng Chem Res 2011;50:11406–21. https://doi.org/10.1021/IE201276M/ASSET/IMAGES/LARGE/IE-2011-01276M_0001.JPEG.

[33] Qi G, Wang S, Yu H, Wardhaugh L, Feron P, Chen C. Development of a rate-based model for CO2 absorption using aqueous NH3 in a packed column. Int J Greenhouse Gas Control 2013;17:450–61. https://doi.org/10.1016/J.IJGGC.2013.05.027.

[34] Yu H, Qi G, Wang S, Morgan S, Allport A, Cottrell A, et al. Results from trialling aqueous ammonia-based post-combustion capture in a pilot plant at Munmorah Power Station: Gas purity and solid precipitation in the stripper. Int J Greenhouse Gas Control 2012;10:15–25. https://doi.org/10.1016/J.IJGGC.2012.04.014.

[35] Hosseinifard F, Hosseinpour M, Salimi M, Amidpour M. Cost-effective solar-driven configurations for post-combustion carbon capture at Abadan Power Plant: MEA, DEA, and DGA absorption-based. Clean Eng Technol 2024;23:100842. https://doi.org/10.1016/J.CLET.2024.100842.

[36] Ding X, Chen H, Li J, Zhou T. Comparative techno-economic analysis of CO2 capture processes using blended amines. Carbon Capture Sci Technol 2023;9:100136. https://doi.org/10.1016/J.CCST.2023.100136.

[37] Mudhasakul S, Ku H, ming, Douglas PL. A simulation model of a CO2 absorption process with methyldiethanolamine solvent and piperazine as an activator. Int J Greenhouse Gas Control 2013;15:134–41. https://doi.org/10.1016/J.IJGGC.2013.01.023.

[38] Garcia M, Knuutila HK, Gu S. ASPEN PLUS simulation model for CO2 removal with MEA: Validation of desorption model with experimental data. J Environ Chem Eng 2017;5:4693–701. https://doi.org/10.1016/J.JECE.2017.08.024.

[39] Kopac T, Demirel Y. Impact of thermodynamics and kinetics on the carbon capture performance of the amine-based CO2 capture system. Environmental Science and Pollution Research 2024 31:27 2024;31:39350–71. https://doi.org/10.1007/S11356-024-33792-Y.

[40] Xiang J, Wei D, Mao W, Liu T, Luo Q, Huang Y, et al. Comprehensive kinetic study of carbon dioxide absorption in blended tertiary/secondary amine solutions: Experiments and simulations. Sep Purif Technol 2024;330:125310. https://doi.org/10.1016/J.SEPPUR.2023.125310.

[41] Yang N, Yu H, Li L, Xu D, Han W, Feron P. Aqueous ammonia-based post-combustion CO2 capture: a Review. Oil Gas Sci Technol 2014. https://doi.org/10.2516/OGST/2013160.

[42] Leonzio G, Zondervan E. Innovative application of statistical analysis for the optimization of CO2 absorption from flue gas with ionic liquid. Computer Aided Chemical Engineering 2019;46:151–6. https://doi.org/10.1016/B978-0-12-818634-3.50026-6.

[43] de Riva J, Ferro V, Moya C, Stadtherr MA, Brennecke JF, Palomar J. Aspen Plus supported analysis of the post-combustion CO2 capture by chemical absorption using the [P2228][CNPyr] and [P66614][CNPyr]AHA Ionic Liquids. Int J Greenhouse Gas Control 2018;78:94–102. https://doi.org/10.1016/J.IJGGC.2018.07.016.

[44] Ferro VR, Moya C, Moreno D, Santiago R, De Riva J, Pedrosa G, et al. Enterprise Ionic Liquids Database (ILUAM) for use in Aspen ONE Programs Suite with COSMO-Based Property Methods. Ind Eng Chem Res 2018;57:980–9. https://doi.org/10.1021/ACS.IECR.7B04031/ASSET/IMAGES/LARGE/IE-2017-04031C_0004.JPEG.

[45] Yu G, Wei Z, Chen K, Guo R, Lei Z. Predictive molecular thermodynamic models for ionic liquids. AIChE J 2022;68:e17575. https://doi.org/10.1002/AIC.17575.

[46] Vega LF, Vilasecaa O, Llovell F, Andreua JS. Modeling ionic liquids and the solubility of gases in them: recent advances and perspectives. Fluid Phase Equilib 2010;294:15–30. https://doi.org/10.1016/J.FLUID.2010.02.006.

[47] Ashkanani HE, Wang R, Shi W, Siefert NS, Thompson RL, Smith K, et al. Levelized cost of CO2 Captured using five Physical Solvents in Pre-combustion applications. Int J Greenhouse Gas Control 2020;101:103135. https://doi.org/10.1016/J.IJGGC.2020.103135.

[48] Sujatha I, Venkatarathnam G. Performance of a vapour absorption heat transformer operating with ionic liquids and ammonia. Energy 2017;141:924–36. https://doi.org/10.1016/J.ENERGY.2017.10.002.

[49] Hospital-Benito D, Lemus J, Moya C, Santiago R, Palomar J. Process analysis overview of ionic liquids on CO2 chemical capture. Chem Eng J 2020;390:124509. https://doi.org/10.1016/J.CEJ.2020.124509.

[50] Ma C, Wang N, Ye N, Ji X. CO2 capture using ionic liquid-based hybrid solvents from experiment to process evaluation. Appl Energy 2021;304:117767. https://doi.org/10.1016/J.APENERGY.2021.117767.

[51] Nguyen TBH, Zondervan E. Ionic Liquid as a Selective Capture Method of CO2 from different sources: Comparison with MEA. ACS Sustain Chem Eng 2018;6:4845–53. https://doi.org/10.1021/ACSSUSCHEMENG.7B04247/ASSET/IMAGES/MEDIUM/SC-2017-04247V_M016.GIF.

[52] Palomar J, Lemus J, Navarro P, Moya C, Santiago R, Hospital-Benito D, et al. Process simulation and Optimization on Ionic Liquids. Chem Rev 2024;124:1649–737. https://doi.org/10.1021/ACS.CHEMREV.3C00512/ASSET/IMAGES/MEDIUM/CR3C00512_0037.GIF.

[53] Tripodi A, Compagnoni M, Bahadori E, Rossetti I. Process simulation of ammonia synthesis over optimized Ru/C catalyst and multibed Fe + Ru configurations. J Ind Eng Chem 2018;66:176–86. https://doi.org/10.1016/J.JIEC.2018.05.027.

[54] Sobol IM. Global sensitivity indices for nonlinear mathematical models and their Monte Carlo estimates. Math Comput Simul 2001;55:271–80. https://doi.org/10.1016/S0378-4754(00)00270-6.

[55] Navid A, Khalilarya S, Abbasi M. Diesel engine optimization with multi-objective performance characteristics by non-evolutionary Nelder-Mead algorithm: Sobol sequence and Latin hypercube sampling methods comparison in DoE process. Fuel 2018;228:349–67. https://doi.org/10.1016/J.FUEL.2018.04.142.

[56] Renardy M, Joslyn LR, Millar JA, Kirschner DE. To Sobol or not to Sobol? the effects of sampling schemes in systems biology applications. Math Biosci 2021;337:108593. https://doi.org/10.1016/J.MBS.2021.108593.

[57] Udara SPRA, Kohilan R, Lakshan MAL, Madalagama MKL, Pathirana PRP, Sandupama PWS. Simulation of carbon dioxide capture for industrial applications. Energy Rep 2020;6:659–63. https://doi.org/10.1016/J.EGYR.2019.11.134.

[58] Vesely L, Kapat J, Macadam S, Thangavel P. Innovative Flue Gas-to-sCO2 Primary Heat Exchanger Design for Cement Plant Waste Heat Recovery. 7th International Supercritical CO2 Power Cycles Symposium, San Antonio: 2022, p. 181.

[59] Song C, Pan W, Srimat ST, Zheng J, Li Y, Wang YH, et al. Tri-reforming of methane over Ni Catalysts for CO2 conversion to Syngas with Desired H2/CO Ratios using Flue Gas of Power Plants without CO2 Separation. Stud Surf Sci Catal 2004;153:315–22. https://doi.org/10.1016/S0167-2991(04)80270-2.

[60] Aouini I, Ledoux A, Estel L, Mary S. Pilot Plant Studies for CO2 Capture from Waste Incinerator Flue Gas using MEA based Solvent. Oil & Gas Science and Technology – Revue d'IFP Energies Nouvelles 2014;69:1091–104. https://doi.org/10.2516/OGST/2013205.

[61] Bui M, Gunawan I, Verheyen TV, Meuleman E. Dynamic operation of liquid absorbent-based post-combustion CO2 capture plants. Absorption-Based Post-Combustion Capture of Carbon Dioxide 2016:589–621. https://doi.org/10.1016/B978-0-08-100514-9.00024-X.

[62] David E, Stanciu V, Sandra C, Armeanu A, Niculescu V. Exhaust Gas Treatment Technologies for Pollutant Emission Abatement from Fossil fuel Power Plants. WIT Trans Ecol Environ 2007;102:923–32. https://doi.org/10.2495/SDP070882.

[63] Subramanian N, Madejski P. Analysis of CO2 capture process from flue-gases in combined cycle gas turbine power plant using post-combustion capture technology. Energy 2023;282:128311. https://doi.org/10.1016/J.ENERGY.2023.128311.

[64] Jana A, Modi A. Recent progress on functional polymeric membranes for CO2 separation from flue gases: a review. Carbon Capture Sci Technol 2024;11:100204. https://doi.org/10.1016/J.CCST.2024.100204.

[65] Baker RW, Freeman B, Kniep J, Huang YI, Merkel TC. CO2 Capture from Cement Plants and Steel Mills using Membranes. Ind Eng Chem Res 2018;57:15963–70. https://doi.org/10.1021/ACS.IECR.8B02574/ASSET/IMAGES/LARGE/IE-2018-02574K_0007.JPEG.

[66] Liang X, Lin Q, Muslemani H, Lei M, Liu Q, Li J, et al. Assessing the Economics of CO2 Capture in China's Iron/Steel Sector: a Case Study. Energy Procedia 2019;158:3715–22. https://doi.org/10.1016/J.EGYPRO.2019.01.886.

[67] Parkhi A, Cremaschi S, Jiang Z. Techno-Economic Analysis of CO2 Capture from Pulp and Paper Mill Limekiln. IFAC-PapersOnLine 2022;55:284–91. https://doi.org/10.1016/J.IFACOL.2022.07.458.

[68] Güleç F, Meredith W, Snape CE. Progress in the CO2 Capture Technologies for Fluid Catalytic Cracking (FCC) Units—A Review. Front Energy Res 2020;8:519098. https://doi.org/10.3389/FENRG.2020.00062/BIBTEX.

[69] Selalame TW, Patel R, Mujtaba IM, John YM. Integration of the FCC unit with amine base post-combustion capture. Energy Convers Manag 2025;344:120242. https://doi.org/10.1016/J.ENCONMAN.2025.120242.

[70] Zhang H, Wang L, Van herle J, Maréchal F, Desideri U. Techno-economic comparison of green ammonia production processes. Appl Energy 2020;259:114135. https://doi.org/10.1016/J.APENERGY.2019.114135.

[71] Adya Zizwan P, Zarlis M, Budhiarti Nababan E, Syakur MA, Khotimah BK, Rochman S, et al. Integration K-Means Clustering Method and Elbow Method for Identification of the best Customer Profile Cluster. IOP Conf Ser. Mater Sci Eng 2018;336:012017. https://doi.org/10.1088/1757-899X/336/1/012017.

[72] Chen Z, Li Y, Chen B, Ma W, Chen L, Xu B. An empirical study on dynamic typing related practices in python systems. IEEE International Conference on Program Comprehension 2020;20:83–93. https://doi.org/10.1145/3387904.3389253.

[73] Mathias PM, Reddy S, O'Connell JP. Quantitative evaluation of the chilled-ammonia process for CO2 capture using thermodynamic analysis and process simulation. Int J Greenhouse Gas Control 2010;4:174–9. https://doi.org/10.1016/J.IJGGC.2009.09.016.

[74] Qi G, Wang S, Yu H, Feron P, Chen C. Rate-based Modeling of CO2 Absorption in Aqueous NH3 in a Packed Column. Energy Procedia 2013;37:1968–76. https://doi.org/10.1016/J.EGYPRO.2013.06.077.

[75] Qin F, Wang S, Hartono A, Svendsen HF, Chen C. Kinetics of CO2 absorption in aqueous ammonia solution. Int J Greenhouse Gas Control 2010;4:729–38. https://doi.org/10.1016/J.IJGGC.2010.04.010.

[76] Fang M, Xiang Q, Yu C, Xia Z, Zhou X, Cai D, et al. Experimental study on CO2 absorption by aqueous ammonia solution at elevated pressure to enhance CO2 absorption and suppress ammonia vaporization. Greenhouse Gases Sci Technol 2015;5:210–21. https://doi.org/10.1002/GHG.1463.

[77] Darde V, Thomsen K, van Well WJM, Stenby EH. Chilled ammonia process for CO2 capture. Int J Greenhouse Gas Control 2010;4:131–6. https://doi.org/10.1016/J.IJGGC.2009.10.005.

[78] Jilvero H. Ammonia-Based Post-Combustion Capture of Carbon Dioxide. Chalmers University of Technology, 2013.

[79] Jilvero H, Normann F, Andersson K, Johnsson F. Ammonia-based post combustion – the techno-economics of controlling ammonia emissions. Int J Greenhouse Gas Control 2015;37:441–50. https://doi.org/10.1016/J.IJGGC.2015.03.039.

[80] Xin K, Gallucci F, van Annaland M, S.. Optimization of solvent properties for post-combustion CO2 capture using process simulation. Int J Greenhouse Gas Control 2020;99:103080. https://doi.org/10.1016/J.IJGGC.2020.103080.

[81] Al Juaied M, Whitmore A. Realistic costs of carbon capture 2009. https://doi.org/10.2172/960194.

[82] Schmelz WJ, Hochman G, Miller KG. Total cost of carbon capture and storage implemented at a regional scale: northeastern and midwestern United States. Interface Focus 2020;10. https://doi.org/10.1098/RSFS.2019.0065.

[83] Anderson S, Newell R. Prospects for carbon capture and storage technologies. Annu Rev Env Resour 2004;29:109–42. https://doi.org/10.1146/ANNUREV.ENERGY.29.082703.145619/CITE/REFWORKS.

[84] David J, Herzog H. The cost of carbon capture. fifth international conference on greenhouse gas control technologies. Cairns 2000.

[85] Rubin ES, Zhai H. The cost of carbon capture and storage for natural gas combined cycle power plants. Environ Sci Technol 2012;46:3076–84. https://doi.org/10.1021/ES204514F/SUPPL_FILE/ES204514F_SI_001.PDF.

[86] Işlegen Ö, Reichelstein S. Carbon Capture by Fossil fuel Power Plants: an Economic Analysis. Manag Sci 2010;57:21–39. https://doi.org/10.1287/MNSC.1100.1268.

[87] Moch JM, Xue W, Holdren JP. Carbon Capture, utilization, and Storage: Technologies and costs in the U.S. Context White House 2022.

[88] Gopal S, Patro K, Kumar ShK. Normalization: a Preprocessing Stage. IARJSET 2015:20–2. https://doi.org/10.17148/iarjset.2015.2305.

[89] Abdi H, Williams LJ. Principal component analysis. Wiley Interdiscip Rev Comput Stat 2010;2:433–59. https://doi.org/10.1002/WICS.101.